EBioMedicine 15 (2017) 193–202

Contents lists available at ScienceDirect

EBioMedicine

journal homepage: www.ebiomedicine.com

Research Paper

Muscle Weakness and Fibrosis Due to Cell Autonomous and Non-cell Autonomous Events in Collagen VI Deficient Congenital Muscular Dystrophy

Satoru Noguchi [a,b,*], Megumu Ogawa [a], May Christine Malicdan [c,d], Ikuya Nonaka [a], Ichizo Nishino [a,b]

[a] Department of Neuromuscular Research, National Institute of Neuroscience, Kodaira, Tokyo, Japan
[b] Department of Clinical Development, Translational Medical Center, National Center of Neurology and Psychiatry, Kodaira, Tokyo, Japan
[c] Medical Genetics Branch, National Human Genome Research Institute, National Institutes of Health, Bethesda, MD, USA
[d] NIH Undiagnosed Diseases Program, Common Fund, Office of the Director, National Institutes of Health, Bethesda, 20892, MD, USA

ARTICLE INFO

Article history:
Received 13 September 2016
Received in revised form 11 December 2016
Accepted 19 December 2016
Available online 23 December 2016

Keywords:
Collagen
Fibrosis
IGF-1
Mesenchymal
Mouse
Muscular dystrophy
Skeletal muscles
Weakness

ABSTRACT

Congenital muscular dystrophies with collagen VI deficiency are inherited muscle disorders with a broad spectrum of clinical presentation and are caused by mutations in one of *COL6A1–3* genes. Muscle pathology is characterized by fiber size variation and increased interstitial fibrosis and adipogenesis. In this study, we define critical events that contribute to muscle weakness and fibrosis in a mouse model with collagen VI deficiency. The *Col6a1*-$^{GT/GT}$ mice develop non-progressive weakness from younger age, accompanied by stunted muscle growth due to reduced IGF-1 signaling activity. In addition, the *Col6a1*$^{GT/GT}$ mice have high numbers of interstitial skeletal muscle mesenchymal progenitor cells, which dramatically increase with repeated myofiber necrosis/regeneration. Our results suggest that impaired neonatal muscle growth and the activation of the mesenchymal cells in skeletal muscles contribute to the pathology of collagen VI deficient muscular dystrophy, and more importantly, provide the insights on the therapeutic strategies for collagen VI deficiency.

© 2016 The Authors. Published by Elsevier B.V. This is an open access article under the CC BY-NC-ND license (http://creativecommons.org/licenses/by-nc-nd/4.0/).

1. Introduction

Primary collagen VI deficiencies due to mutations in *COL6A1*, *COL6A2* and *COL6A3* lead to either a severe, Ullrich congenital muscular dystrophy (UCMD, MIM 254090) or a mild, Bethlem myopathy (BTHLM1, MIM 158810) (Allamand et al., 2011). UCMD is clinically characterized by muscle weakness, respiratory failure, proximal joint contracture, and scoliosis (Nonaka et al., 1981; Ullrich, 1930). UCMD muscle pathology shows marked variation in fiber size, scattered muscle necrosis and regeneration, and increased endomysial fibrosis and adipogenesis. The prevalence of UCMD has been reported to be 1.3 per million in northern England (Norwood et al., 2009), while primary collagen VI deficiencies are the second most common congenital muscular dystrophy in Japan (Okada et al., 2007). Autosomal recessive forms are caused by homozygous or compound heterozygous null or frame-shift mutations in *COL6A1*, *COL6A2* and *COL6A3* genes, while the autosomal dominant or sporadic forms are caused by heterozygous missense mutation of glycine, in-frame exon deletion or in-frame splicing mutation in the region that encodes triple helical domain of type VI collagen (Baker et al., 2005; Higuchi et al., 2001; Ishikawa et al., 2004). Natural history studies on UCMD in Japan showed that sporadic cases account for 85% of the total UCMD cohort, but both recessive and sporadic UCMD patients share similar clinical course and symptoms (Yonekawa et al., 2013). To date, there is no approved pharmacological therapy for primary collagen VI deficiency, as the mechanism of disease has not been fully elucidated.

Previous studies using samples from *Col6a1*-KO mice (Bonaldo et al., 1998) and patients suggested that impaired mitochondrial function and autophagy dysfunction largely contributed to disease progression (Angelin et al., 2007; Grumati et al., 2010; Irwin et al., 2003), and led to a clinical trial evaluating low protein diet to reactivate autophagy in BTHLM1/UCMD patients (https://clinicaltrials.gov/, NCT01438788). Impaired mitophagy and autophagy, however, could not fully explain why loss of extracellular collagen VI can cause problems within the intracellular milieu, including the changes in pathology that are commonly seen in collagen VI deficient muscles, necessitating further investigation on the mechanism of disease.

Braghetta et al. have identified a muscle-specific enhancer at −1.4-kb upstream of the *Col6a1* gene in mice and analyzed spatiotemporal expression of *Col6a1* during mouse embryonic development (Braghetta et al., 1996, 2008) and showed that *Col6a1*-expressing cells were not myofibers, but were actually interstitial mesenchymal cells

* Corresponding author at: Department of Neuromuscular Research, National Institute of Neuroscience, Kodaira, Tokyo, Japan.
E-mail address: noguchi@ncnp.go.jp (S. Noguchi).

http://dx.doi.org/10.1016/j.ebiom.2016.12.011
2352-3964/© 2016 The Authors. Published by Elsevier B.V. This is an open access article under the CC BY-NC-ND license (http://creativecommons.org/licenses/by-nc-nd/4.0/).

that gradually decremented in number postnally. These results suggest that collagen VI expression is transcriptionally regulated during development and in addition activated under the influence of factors released myoblasts. In this study, we show that muscle weakness in mice lacking collagen VI (*Col6a1*$^{GT/GT}$) was due to reduced number of myofibers, resulting to an overall decrease in muscle size. We also demonstrated that the number of mesenchymal progenitor cells (MPCs) is surprisingly increased and contributed to endomysial fibrosis in the skeletal muscles of older *Col6a1*$^{GT/GT}$ mice. Our study provides the insights in the pathomechanism of the primary collagen VI deficiencies.

2. Materials and Methods

2.1. Mice

The hypomorph model of *Col6a1* deficiency resulted from an attempt to generate KI mice with a point mutation of G283R in *Col6a1* genes. These mice were generated using ES cells with homologous recombination as shown in Fig. S1. Targeting vector construction, homologous recombination in ES cells, generation of chimera mice and heterozygous mice are performed by Ingenious Targeting Laboratory. We backcrossed the mutated mice in the C57BL/6J strain for at least eight generations. Mice were maintained in a barrier-free, specific pathogen-free grade facility on a 12-h light, 12-h dark cycle and had free access to normal chow and water. All animal experiments conducted in this study were approved by and carried out within the rules and regulations of the Ethical Review Committee on the Care and Use of Rodents in the National Institute of Neuroscience, National Center of Neurology and Psychiatry. These policies are based on the "Guideline for Animal Experimentation" as sanctioned by the Council of the Japanese Association of Laboratory Animal Science.

2.2. Patients' Muscles

The ethics committee of the National Center of Neurology and Psychiatry approved this study and the use of human subjects for this study. Biopsied muscles from UCMD patients diagnosed based on clinical features, muscle pathology and genetic test (UCMD1: patient 2 (Yonekawa et al., 2013), compound heterozygous mutations: c.5692delG/c.8737delG in *COL6A3*; UCMD2: patient 14 (Yonekawa et al., 2013), heterozygous mutation: c.812G>A in *COL6A2*; for electron microscopic observation: patient 1 in ref. 9, compound heterozygous mutations: c.1771-3G>C/c.1270-1G>C in *COL6A2*), and diseased control patient, were obtained with informed consent.

2.3. Motor Performance and Muscle Contraction Force Measurements

Grip strength of combined forelimbs/hindlimbs was measured by five successive trials using a MK-380M grip strength meter (Muromachi kikai). Voluntary exercise within an individual cage was measured using running wheel (SW-15 and CIF3Win) for 1 week as described previously (Yonekawa et al., 2014). Measurement of the contractile properties of TA and gastrocnemius muscles was performed according to the previous protocols (Malicdan et al., 2009a). *Col6a1*$^{GT/GT}$ and control littermates ($n = 3$–7 mice: grip test and $n = 5$–6 mice: force measurement, per gender) were measured at 14, 22, 30, 39 and 60 weeks of ages.

2.4. Histological Analysis of TA Muscles

After measurement of force, the mice were euthanized and the muscle tissues were processed and kept at −80 °C until use (Yonekawa et al., 2014). For measurement of fiber diameter, fiber number and membrane indentation in myofibers, we stained the sarcolemma of myofibers on muscle cryosections with anti-caveolin3 antibody (Santa Cruz, dilution: 1:200) for 1 h followed by Alexa Fluor-conjugated donkey IgG against goat IgG (Invitrogen, 1:800) for 30 min and took the pictures with a BZ X-700 microscope (Keyence). Diameters of 2300–6000 myofibers were measured with ImageJ software (National Institute of Health) (Malicdan et al., 2009a). Total fiber number and fibers with membrane indentation were counted in whole sections. For MPC counting, we stained the MPCs with anti-PDGFRα antibody (R&D, 1:200) and laminin with anti-laminin α2 antibody (ALEXIS, 1:200) for 1 h followed by staining with Alexa Fluor-conjugated secondary antibody. For fibrosis, we stained the sections with anti-collagen III antibody (LSL, 1:200) for 1 h followed by staining with Alexa Fluor-conjugated secondary antibody and measured the stained area with hybrid cell count software on BZ X-700 microscope (Keyence). Other antibodies used in this study were anti-collagen VI (LSL, 1:100), anti-collagen IV (Medac, 1:100), anti-MyoD (Santa Cruz, 1:100), Tcf4 (Cell Signaling Technologies, 1:100), anti-smooth muscle actin (Sigma, 1:100), and anti-Pax7 (Developmental Studies Hybridoma Bank). For electron microscopic observation, the samples of human muscles were processed by standard protocol (Malicdan et al., 2009b).

2.5. ELISA

Blood IGF-1 was measured by using IGF1 Mouse ELISA Kit (Abcam) and Absorbance Microplate Reader MTP-310Lab (CORONA).

2.6. CTXi

To induce muscle regeneration, we injected cardiotoxin into muscles of *Col6a1*$^{GT/GT}$ mice as previously reported (Hosaka et al., 2002). Briefly, 7 μg of cardiotoxin (Sigma) per muscle once was injected into tibialis anterior muscles 1–3 times with a 4-week interval and then muscle was examined and harvested at 24 weeks of age according to the schedule described in Fig. 6a. For monitoring the proliferating cells, on 1 or 3 days after CTXi, 0.6–0.9 mg EdU/mouse was intraperitoneally injected 2 h before muscle harvest. Detection of incorporated EdU was done by Click-it EdU Imaging Kit (Invitrogen).

2.7. Blood Glucose Measurement

Blood glucose level from tail vein was measured by using Accu-Chek ST Meter (Roche).

2.8. Preparation of MPCs

MPCs were prepared from CTX-treated TA muscles of *Col6a1*$^{GT/GT}$ and LM mice according to previous report (Heredia et al., 2013). Briefly, isolated muscles were digested with 0.05% Collagenase Type 2 and 0.1% Dispase (Gibco) in DMEM for 30 min at 37 C. Liberated cells were passed through Cell Strainer and collected by centrifugation. MPCs were purified by depletion of endothelial cells, leukocytes, and muscle cells using a mixture of biotin-conjugated anti-CD31, anti-CD45, and anti-α7 integrin antibodies, respectively (Miltenyi Biotec) and then streptavidin magnetic beads (Miltenyi Biotec). The flow through fraction was collected and confirmed by immunostaining for PDGFRα.

2.9. Western Blotting

Phosphorylated proteins were prepared from skeletal muscle cryosections with some modifications according to the previous report (Yonekawa et al., 2014). Proteins were extracted in 1% Triton X-100/Tris buffered saline in the presence of 1 mM Na_3VO_4, 10 mM NaF and protein inhibitor cocktail (Roche). SDS-PAGE was done following Laemmli's method. Membranes were incubated with the following antibodies: anti-collagen VI (Santa Cruz, 1:250), anti-tubulin (Sigma, 1:250), anti-Akt1 (CST, 1:1000), anti-S473 phosphoAkt (CST, 1:200), anti-p70S6 kinase (Santa Cruz, 1:200), anti-S411 phosphoS6 kinase (Santa Cruz, 1:200), and anti-T421/S424 phosphoS6kinase (Santa Cruz, 1:200). After washing, membranes were incubated in appropriate

HRP-labeled secondary antibodies, washed, and then made to react with Immobilon Western Chemiluminescent HRP Substrate. Detection and quantification of band intensities were done by ImageQuant LAS 4000 system (GE healthcare).

2.10. Data Analysis

All values were expressed as means ± SEM. The paired *t*-test was used for statistical significance. A *p* value of 0.05 was considered as the threshold for significance.

3. Results

3.1. Collagen VI Deficient Mouse Exhibits Non-progressive Muscle Weakness and Impaired Muscle Growth

We generated a hypomorphic mouse following an attempt to generate a knockin model that expressed a c. 847A>G (p.G283R) mutation in exon 9 of the *Col6a1* gene and the *neo* cassette in intron 9 (Fig. S1). Mice heterozygous at the genomic level of the knockin allele were indistinguishable with wild type control; heterozygous breeding pairs produced litters with Mendelian genotype distribution. Mice homozygous for the knockin allele (KI/KI) were not lethal but were remarkably smaller than control littermates (LM). Analysis of mRNA expression showed marked reduction in *Col6a1* levels and only aberrant spliced products from exon 9 to the *neo* cassette (KI/KI in Fig. 1a), suggesting that the knockin variant may have led to a frame-shift after exon 9 (Fig. 1b). Collagen VI was not detected in all of tissues on immunohistochemistry (Fig. 1c) and Western blotting (Fig. 1d) in our mice homozygous for the knockin allele; thus the KI/KI are actually hypomorphs and not true knockins, and from here on referred to as *Col6a1*$^{GT/GT}$.

The *Col6a1*$^{GT/GT}$ mice were smaller in body weight throughout their life (Fig. 2a–b) as compared to control littermates (LM). There are no apparent abnormalities in bone, joint and skin. Analysis of grip test showed limb muscle weakness after 14 weeks of age, but this weakness was not progressive (Fig. 2c–d). Measurement of voluntary locomotion was also reduced in the *Col6a1*$^{GT/GT}$ mice (Fig. 2e and Fig. S2). Tibialis anterior (TA) muscle contractile forces, including twitch and tetanic contractions, were lower in the mutant mice as compared to LM (Fig. 2f–g) and it is likely that this is due to decreased muscle size and cross-sectional areas (Fig. 2h). Specific forces were, however also reduced in twitch contraction in *Col6a1*$^{GT/GT}$ mice (Fig. 2i–j), indicating that collagen VI deficiency not only affects muscle size, but also affects the intrinsic skeletal muscle property including tetanus/twitch rate (Fig. 2k). The contractile properties of gastrocnemius muscles were similarly affected (Fig. S3a—f). These results suggest that *Col6a1*$^{GT/GT}$ mice display a non-progressive mild muscle weakness.

3.2. Impaired Muscle Growth in Collagen VI Deficient Mouse is Associated With Defects in IGF-1 Signaling

For further experiments, all analyses were done using TA muscles. At 30 weeks of age, muscles in *Col6a1*$^{GT/GT}$ appear smaller (Fig. 3a–b), and have rare or no dystrophic changes, necrosis, or centrally-placed nuclei. The pattern of muscle weight in *Col6a1*$^{GT/GT}$ and control littermates (Fig. 3c) followed the pattern of body weight (Fig. 2a–b), whereby a plateau

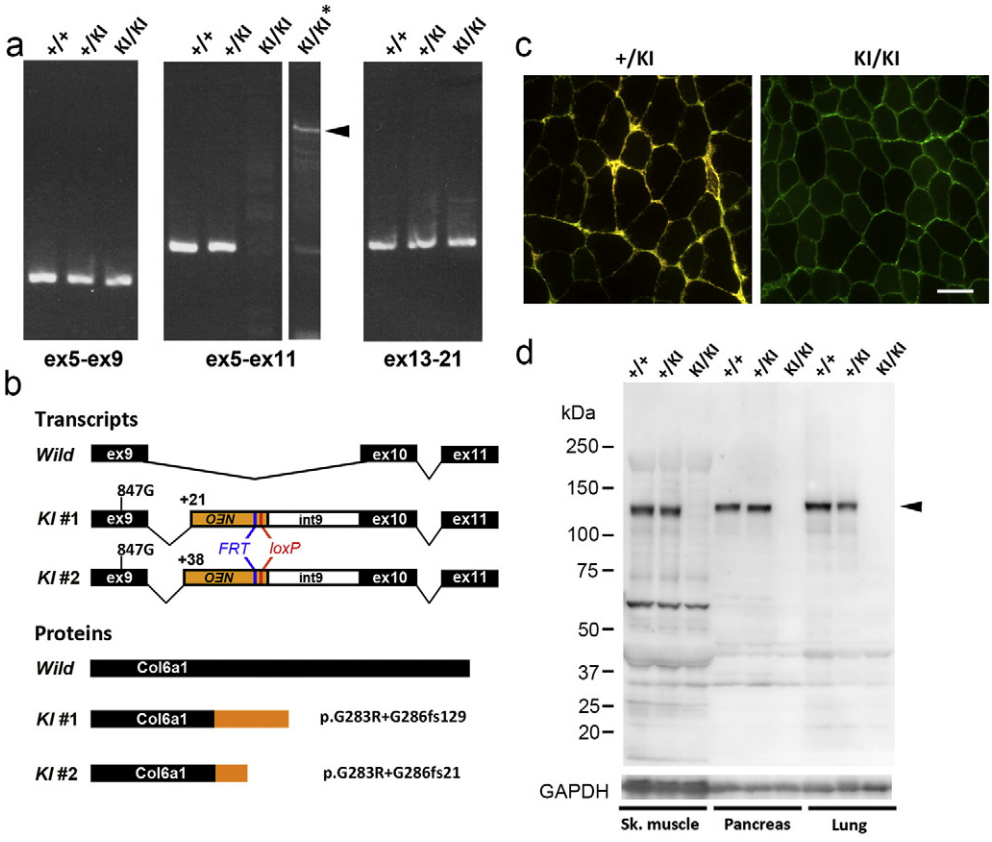

Fig. 1. Generation of *Col6a1* mutated mice. (a) Analysis of *Col6a1* transcripts from wild-type (+/+), heterozygote (+/KI) and homozygote (KI/KI), both of which are harboring knockin allele, by RT-PCR. Left, fragments amplified with primers in exon 5 and exon 9; middle, fragments amplified with primers in exon 5 and exon 11; right, fragments amplified with primers in exon 13 and exon 21. *KI/KI denotes the result by PCR amplification with long extension time. Homozygote gave a longer product with primers in exon 5 and exon 11 (arrowhead). (b) Structure of the two transcripts, #1 and #2, by amplification with primers in exon 5 and exon 11 in homozygote. Both transcripts were predicted to produce truncated proteins by aberrant splicing to *neo* cassette. (c) Expression of collagen VI (red) in the skeletal muscles of homozygotes (KI/KI) is undetectable, while collagen IV (green) is expressed normally in heterozygotes (+/KI). Bar denotes 50 μm. (d) Western blot also showed no expression of collagen VI in various tissues. Arrowhead marks the expected collagen VI band. GAPDH is an endogenous marker.

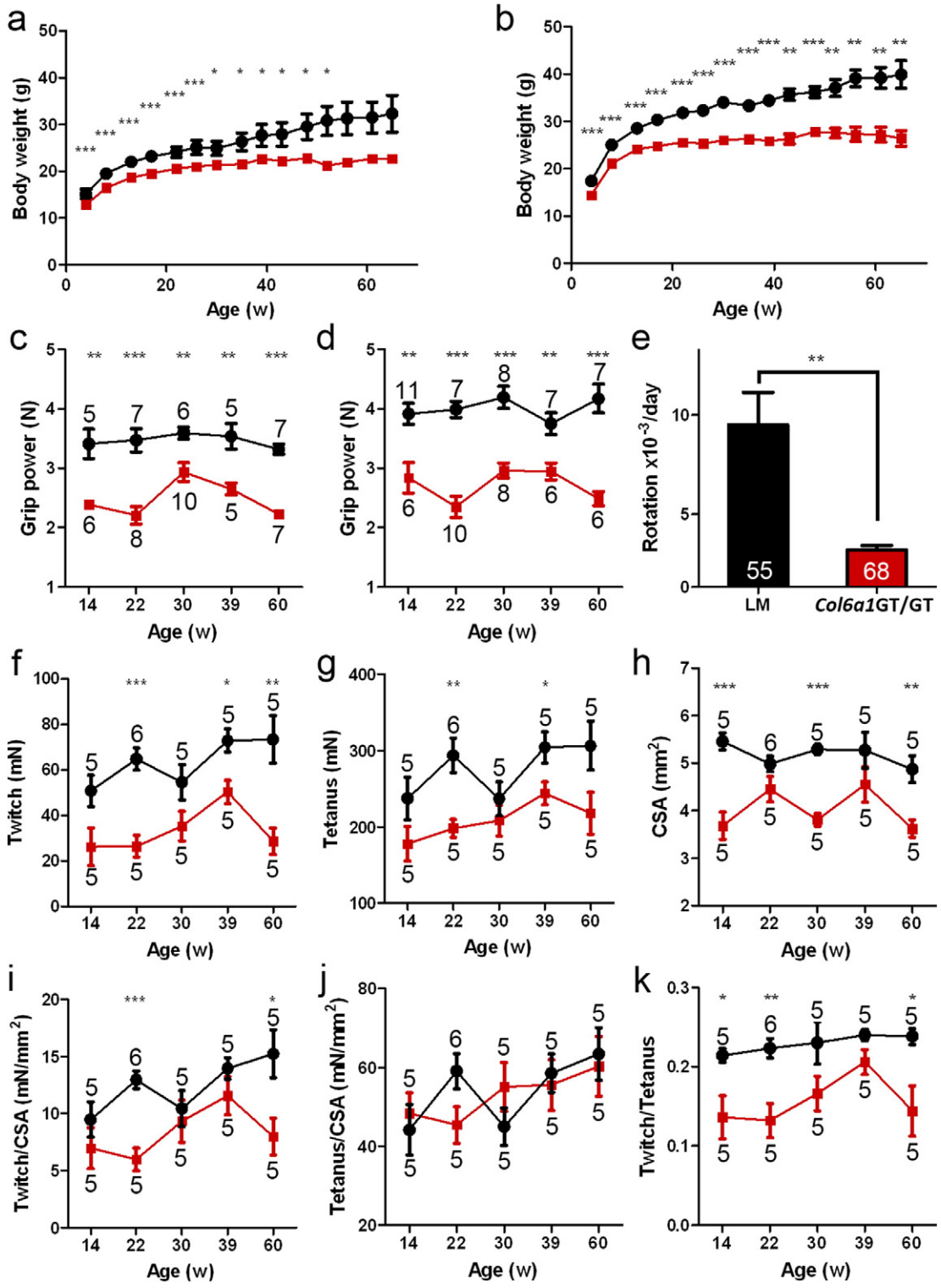

Fig. 2. Overall phenotype of the *Col6a1*$^{GT/GT}$ mice. (a) Growth curves of female: control littermates (black, $n = 5$–113 per aged group) and *Col6a1*$^{GT/GT}$ (red, $n = 5$–54 per aged group). (b) Growth curves of male: control littermates (black, $n = 5$–114 per aged group) and *Col6a1*$^{GT/GT}$ (red, $n = 5$–59 per aged group). (c) Grip power of female: control littermates (black, $n = 5$–10 per aged group) and *Col6a1*$^{GT/GT}$ (red, $n = 5$–8 per aged group). (d) Grip power of male: control littermates (black, $n = 7$–11 per aged group) and *Col6a1*$^{GT/GT}$ (red, $n = 6$–10 per aged group). (e) Voluntary wheel running (rotation per day) of control littermates (black, $n = 28$) and *Col6a1*$^{GT/GT}$ (red, $n = 28$). Contractile properties of TA muscles of LM (black, $n = 5$ per aged group) and *Col6a1*$^{GT/GT}$ (red, $n = 5$ per aged group); (f) peak isometric twitch, (g) maximal tetanic force, (h) cross-sectional area (CSA), (i) specific isometric twitch, (j) specific tetanic force, (k) twitch/tetanus ratio. Data represent the mean ± SEM. $^{*}p < 0.05$, $^{**}p < 0.01$, $^{***}p < 0.001$ on the paired *t*-test were used. Numbers in graphs represent *n* for each data point.

was seen in the *Col6a1*$^{GT/GT}$ after 20 weeks of age. Measurement of the individual myofiber diameter showed no difference in average between *Col6a1*$^{GT/GT}$ and LM (Fig. 3d), but the myofibers <15 μm were increased in *Col6a1*$^{GT/GT}$ mice (Fig. 3d). Surprisingly, in the muscles of *Col6a1*$^{GT/GT}$ mice, we noted a reduction in the total number of myofibers after 3 weeks of age, while at postnatal day 1 there was no difference between the mutant and LM (Fig. 3e. Fig. S4a), suggesting a lag in myofiber number increment. We also found that the number of myonuclei per

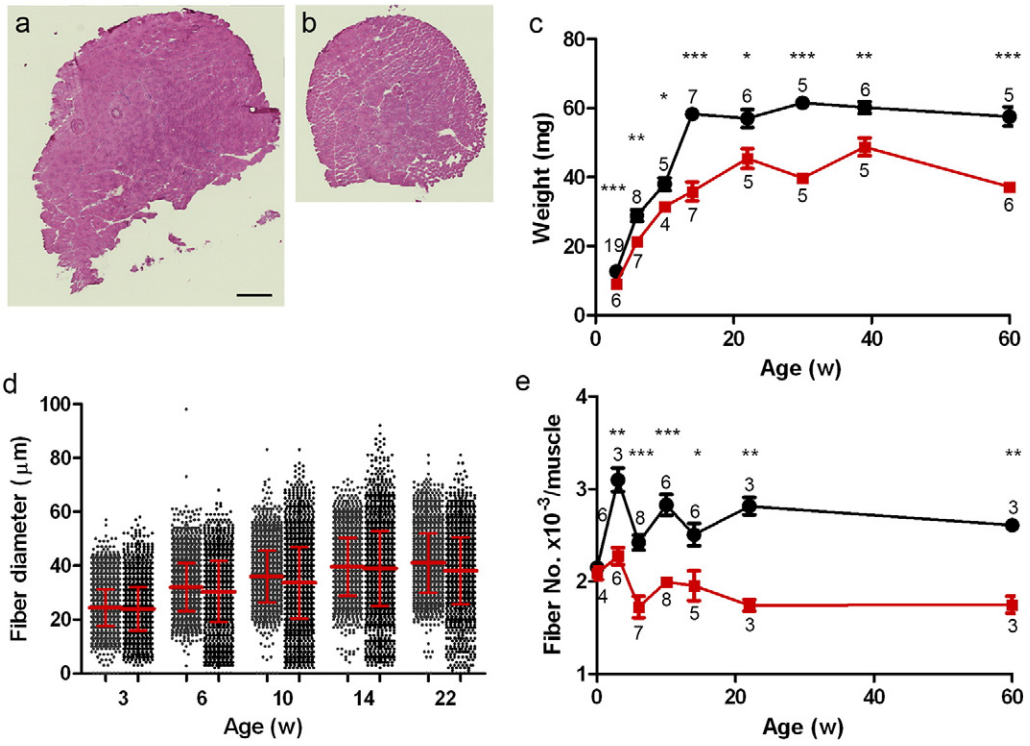

Fig. 3. Histological examination of TA muscles. Appearance of TA muscles in control LM (a) and *Col6a1*$^{GT/GT}$ (b). Bar denotes 500 μm. Necrotic and regenerating fibers are rare. (c) TA muscle weights of control LM (black, $n = 5$–19) and *Col6a1*$^{GT/GT}$ (red, $n = 4$–7). (d) Distribution of myofiber diameter in control LM (gray in left, $n = 2400$–6100) and *Col6a1*$^{GT/GT}$ (black, $n = 2300$–4100). (e) Total fiber number in TA muscle of control LM (black, $n = 3$–8) and *Col6a1*$^{GT/GT}$ (red, $n = 3$–8). Data represent the mean ± SEM. $^{*}p < 0.05$, $^{**}p < 0.01$, $^{***}p < 0.001$ on the paired *t*-test were used. Numbers in graph represent *n* for each data point.

myofiber is higher in *Col6a1*$^{GT/GT}$, however total number of myonuclei in TA muscle of *Col6a1*$^{GT/GT}$ mice was similar in *Col6a1*$^{GT/GT}$ and LM (Fig. S4b—c). Further analysis of the myofiber in different ages of mice revealed that indentation of myofibers was fewer in *Col6a1*$^{GT/GT}$ (Fig. S4d) and the lag in increment of myofibers starts at day 15 (Fig. 4a) indicating a probable defect in muscle growth and signaling during postnatal development.

We then investigated IGF-1, one of the molecules considered to influence myofiber number in skeletal muscle during postnatal development (Holt et al., 2012); as we have suspected that serum IGF-1 level of *Col6a1*$^{GT/GT}$ mice was 80% those of LMs at 15 days of age (Fig. 4b). As expected the downstream kinases to IGF-1 signaling, Akt-1 and p70S6, were less activated in skeletal muscles of *Col6a1*$^{GT/GT}$ mice compared to LM (Fig. 4c–d), suggesting that IGF-1 signaling in neonatal muscle development was impaired in collagen VI deficiency. The observation that the *Col6a1*$^{GT/GT}$ mice had impaired glucose tolerance without insulin resistance (Fig. S5a—b) supports defects in IGF-1 signaling.

3.3. The Number of MPCs is Remarkably Increased in Skeletal Muscles of *Col6a1*$^{GT/GT}$ Mice and UCMD Patients

Other histological findings include fiber size variation and endomysial fibrosis, which were notable after 20 weeks of age (Fig. 5a–c). We then examined the status of MPCs, which were shown to be a source of collagen VI in skeletal muscles (Ito et al., 2013). We confirmed that MPCs from *Col6a1*$^{GT/GT}$ mice did not express collagen VI in cytosol without ascorbic acid (Fig. S6a) and did not secrete collagen VI extracellularly with ascorbic acid (Fig. S6b). We then hypothesized that MPC defects can play a role in collagen VI deficient myopathies, and analyzed PDGFRα-positive MPC, which is implicated in fibrosis and adipogenesis. In LM muscles, the number of MPCs was highest at birth and then remarkably decreased by 6 week of age (lower panels in Fig. 5d). After that, the number of MPCs was constant per area (Fig. 5e). In contrast, the number of MPCs in *Col6a1*$^{GT/GT}$ mice, remained high (three times as much as control) even at 30 weeks of age (Fig. 5d–e); the identity of MPCs was verified by positive Tcf4 staining (Fig. S7), which has been shown to be a specific marker for MPC (Mathew et al., 2011). Intrigued with this finding, we analyzed skeletal muscles of UCMD patients and saw an increase of MPCs especially in the area of endomysial fibrosis (Fig. 5f), indicating that MPCs may contribute to the formation of fibrous tissues in collagen VI deficient patients.

We also noted changes in MPC morphology in collagen VI deficient mice and patients. Normally, as seen in LM mice, MPCs have a round or ovoid shape with almost no cytoplasmic content and are found almost juxtaposed to the basement membrane surrounding myofibers; in *Col6a1*$^{GT/GT}$ muscles, the MPCs are elongated and detached from the basement membrane (upper panels in Fig. 5g). Similarly, the MPCs in UCMD patients appear elongated (lower panels in Fig. 5g), and this was supported by ultrastructural analysis (Fig. S8a—c). MPCs, however, did not appear to be proliferating, because they were not stained with Ki67 antibody and IL-6 levels were increased only in 2–2.5 times in *Col6a1*$^{GT/GT}$ muscles (data not shown).

3.4. Induction of Tissue Injury and Repair Unravels Defects in MPC Activation in *Col6a1*$^{GT/GT}$

To further explore the role of MPCs in collagen VI deficiency, we artificially induced multiple cycles of necrosis/regeneration by intramuscular cardiotoxin injections (CTXi) (Fig. 6a). Following CTXi to muscles, we observed proliferation of PDGFRα-positive MPCs with myofiber necrosis, before starting of myofiber regeneration (data not shown). After three doses of CTXi given in a weekly interval, the *Col6a1*-$^{GT/GT}$ mice displayed marked fiber size variation and endomysial fibrosis (upper panels in Fig. 6b), findings that are similar to the muscle histology of UCMD patients. No delay or defects in muscle regeneration process were observed in *Col6a1*$^{GT/GT}$ mice even with multiple CTXi.

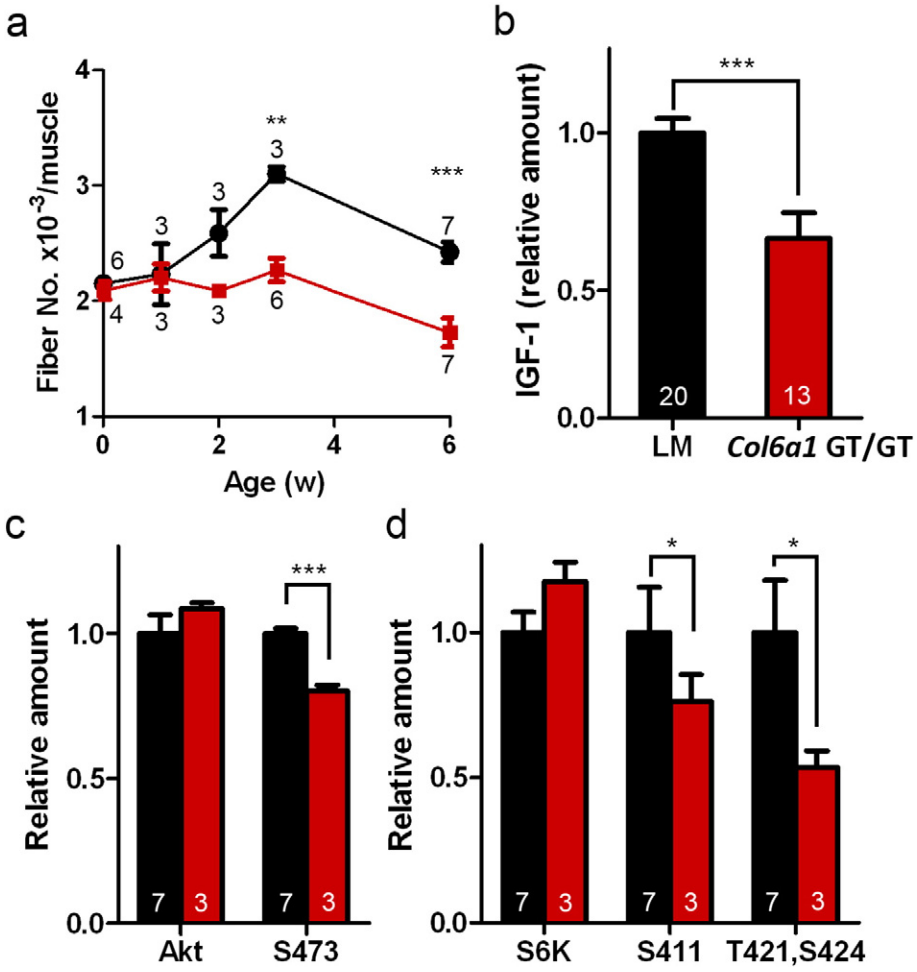

Fig. 4. IGF-1 signaling in neonatal muscle was impaired in *Col6a1*$^{GT/GT}$ mice. (a) Increase in fiber number in TA muscle of control LM (black, $n = 3$–8) and *Col6a1*$^{GT/GT}$ (red, $n = 3$–7) during neonatal period. (b) Serum IGF-1 level. IGF-1 levels of the mice were normalized among each littermate and calculated as ratios to an average level in control LM. (c) Activation of Akt-1 in TA muscles. The amount of Akt-1 was normalized by that of tubulin (Akt). Phosphorylation at S473 of Akt-1 was normalized by total Akt-1 (S473). Control LM (black, $n = 7$) and *Col6a1*$^{GT/GT}$ (red, $n = 3$). (d) Activation of p70S6 kinase in TA muscles. The amount of p70S6 kinase was normalized by that of tubulin (S6K). Phosphorylation at S411 and T421/S424 was normalized by the amount of total p70S6 kinase (S411 and T421, S424). Control LM (black, $n = 7$) and *Col6a1*$^{GT/GT}$ (red, $n = 3$). Data represent the mean ± SEM. $^{*}p < 0.05$, $^{**}p < 0.01$, $^{***}p < 0.001$ on the paired *t*-test were used. Numbers in graphs represent *n* for each data point.

Muscle-retained MPCs, however, were dramatically increased after 3 cycles of CTXi (lower panels in Fig. 6b). In the interstitial area, MPCs appeared elongated and branched on collagen III matrix (data not shown). Multiple CTXi also led to a deterioration of the contractile properties and size of TA muscles in *Col6a*$^{GT/GT}$ mice, while this led to the opposite observation in LM (Fig. 6c–f). Interestingly the number of myofiber after repeated CTXi remained constant in *Col6a1*$^{GT/GT}$ muscles, while hyperplasia and pseudohypertrophy leading to increase in myofiber number were induced in control LM muscles (Fig. 6f).

We further monitored the activation of MPCs in CTXi-induced necrosis/regeneration in *Col6a1*$^{GT/GT}$ muscles by inducing additional muscle injury; CTXi was done in mice already given 3 doses of CTX (CTX3), and compared to CTX-naïve mice (CTX0). After day 1, number of EdU-labeled PDGFRα-positive MPCs was notably increased in *Col6a1*$^{GT/GT}$ but was much higher in CTX3 muscles (upper panels in Fig. 7) as compared to LM. On day 3 after muscle injury, MPCs were observed almost exclusively within the myofibers (Fig. 7, middle panels). Interestingly similar numbers of EdU-labeled MyoD-positive (Fig. 7, bottom panels) and Pax7-positive (data not shown) cells were observed in muscles of *Col6a1*$^{GT/GT}$ mice and LM, suggesting that there is no abnormality in activation of satellite cells.

4. Discussion

Our hypomorphic collagen VI mouse model recapitulates the histological changes in the muscles of UCMD patients and displays non progressive muscle weakness, small muscle mass, fiber size variation, and endomysial fibrosis. The hypomorph status in mice was probably caused by a splicing event due to the insertion of the *neo* cassette, because the cryptic splicing acceptor sites were generated in *neo* cassette (Fig. 1). In contrast to previous studies (Bonaldo et al., 1998), we only observed few necrotic fibers and less pronounced apoptosis. When we performed TUNEL assay in muscle sections of *Col6a1*$^{GT/GT}$ mice and control mice at 12 weeks, we did not detect any positive signals (data not shown). Thus the small muscle mass that we observe is not due to fiber atrophy or necrosis/apoptosis, but is most likely the result of the defective increment of myofiber number during neonatal age.

We identified two critical events that might be associated with pathomechanism collagen VI deficiency in our mice. The first event is a non-cell-autonomous effect from the collagen VI deficiency, causing the dysregulation in the number of myofibers in a muscle. In normal control mice, myofibers increase in number during neonatal growth period until 3 weeks of age. During this period is also the time when

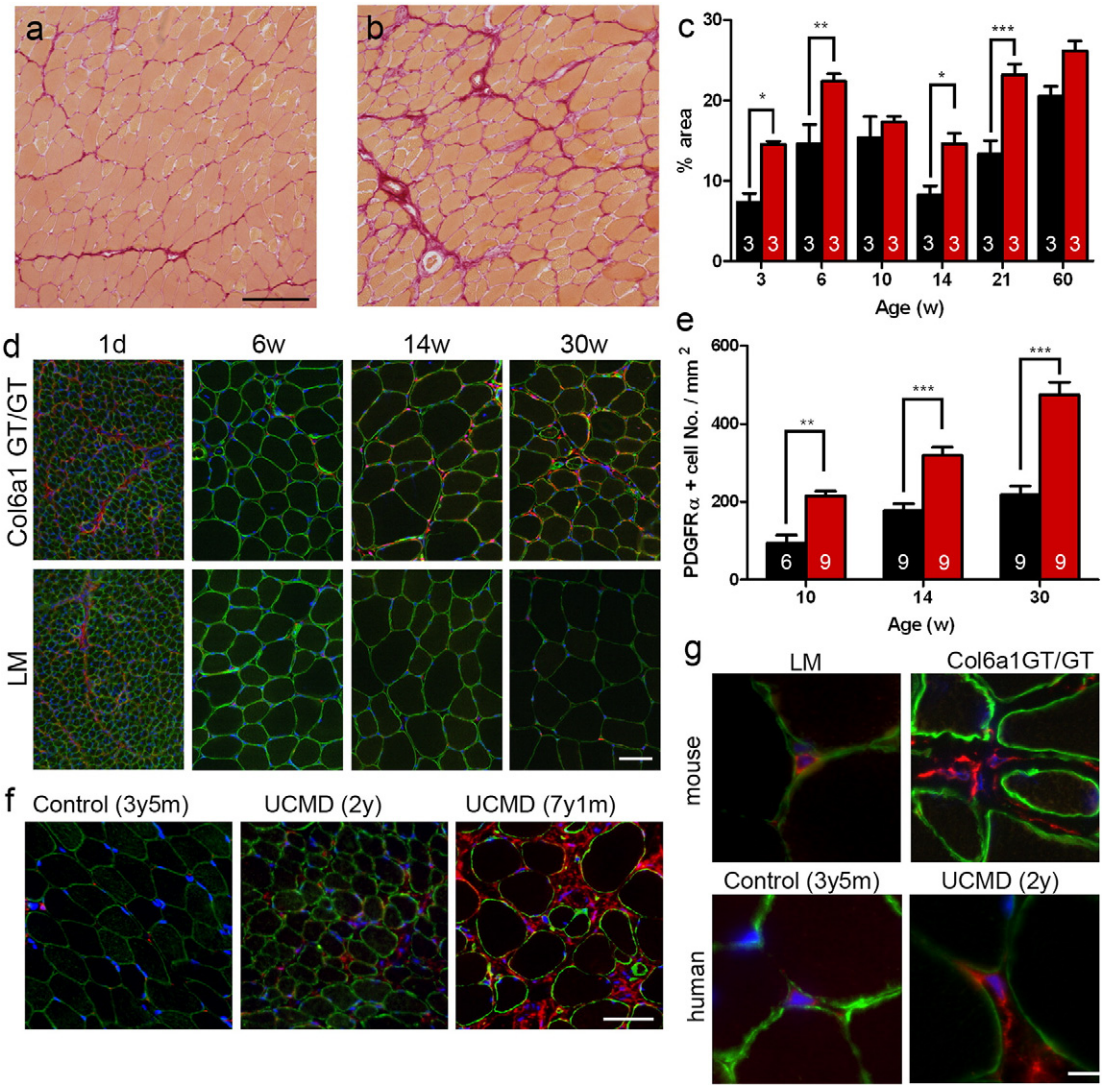

Fig. 5. Fibrosis was remarkable in adult *Col6a1*$^{GT/GT}$ mice. (a and b) Sirius red staining in TA muscles in *Col6a1*$^{GT/GT}$ (b) compared to those in control LM (a). Bar denotes 100 μm. (c) Fibrosis area in control LM (black, $n = 3$) and *Col6a1*$^{GT/GT}$ (red, $n = 3$) in the represented ages. (d) Increase of PDGFRα-positive MPCs in TA muscles of *Col6a1*$^{GT/GT}$. PDGFRα in red; laminin α2 in green. Bar denotes 50 μm. (e) Number of MPCs normalized in area. Control LM (black, $n = 9$) and *Col6a1*$^{GT/GT}$ (red, $n = 6$–9). (f) Increase of PDGFRα-positive MPCs in UCMD muscles. Control, age-matched disease control. Ages at biopsy of patients showed in parentheses. Bar denotes 50 μm. (g) Morphology of MPCs in mice and human muscles. PDGFRα in red; laminin α2 in green; DAPI in blue. Bar denotes 10 μm. Data represent the mean ± SEM. $^{*}p < 0.05$, $^{**}p < 0.01$, $^{***}p < 0.001$ on the paired *t*-test were used. Numbers in graphs represent *n* for each data point.

skeletal muscles have reached reconstitution of extracellular matrix, in parallel with muscle growth, before building up robust and endurable contractile structures in mature muscle. In our model, total number of myonuclei within myofibers in a whole section was not decreased (Fig. 4c) suggesting that the cells, which involved in muscle construction (myogenic cells), were not affected. We also observed the decreased number of membrane indentation within myofibers in *Col6a1*$^{GT/GT}$ muscles in 2 weeks of age (Fig. 4d). These findings clearly suggest that the dysregulation in the myofiber number in collagen VI deficient muscle may be not due to a reduction of the number of myogenic cells, but due to a defect in myofiber splitting/branching which would then lead to an increment of myofiber number.

We demonstrated that the IGF-1 signaling pathway is insufficiently activated, leading to lower serum IGF-1 levels and impaired activation of downstream signaling. It has been only reported that Grb10 is a determinant factor for the number of myofibers in a muscle (Holt et al., 2012). Grb10 is an adaptor protein that links the receptor tyrosine kinase to downstream signal mediators on IGF-1 signaling, and negatively regulates the IGF signaling by enhancing the internalization and degradation of the receptor kinase (Vecchione et al., 2003). Our finding of the insufficient activation of IGF-1 signaling pathway in *Col6a1*$^{GT/GT}$ muscle during perinatal development may suggest that the impairment of growth factor-mediated signal transduction leads to defects in myofiber growth and splitting resulted in fewer myofiber numbers.

The second event is a cell-autonomous influence by skeletal muscle-resident MPCs in promoting interstitial fibrosis. PDGFRα-positive MPCs produce fibrosis and ectopic fat tissue at the late stage of muscular dystrophy (Uezumi et al., 2010, 2011), can be a source of extracellular matrix proteins in skeletal muscles (Ito et al., 2013), and can provide the environment "normal muscle niche" for myofibers (Joe et al., 2010). In this study, we characterized PDGFRα-positive MPCs as a source of collagen VI which may be comparable to the fibroblastic cells identified as an origin of collagen VI in human muscles and also as being positive for some fibroblastic markers, vimentin and FAP, fibroblast activation protein (data not shown). In both *Col6a1*$^{GT/GT}$ mice and human UCMD muscles, we observed that there is a lot of MPCs with elongated morphology; moreover, the MPCs in *Col6a1*$^{GT/GT}$ mice can rapidly proliferate and contribute to fibrosis in response to CTXi on muscle necrosis. Spontaneous activation of MPC in collagen VI deficiency remains to be clarified, because we did not find alteration of IL-4 expression in

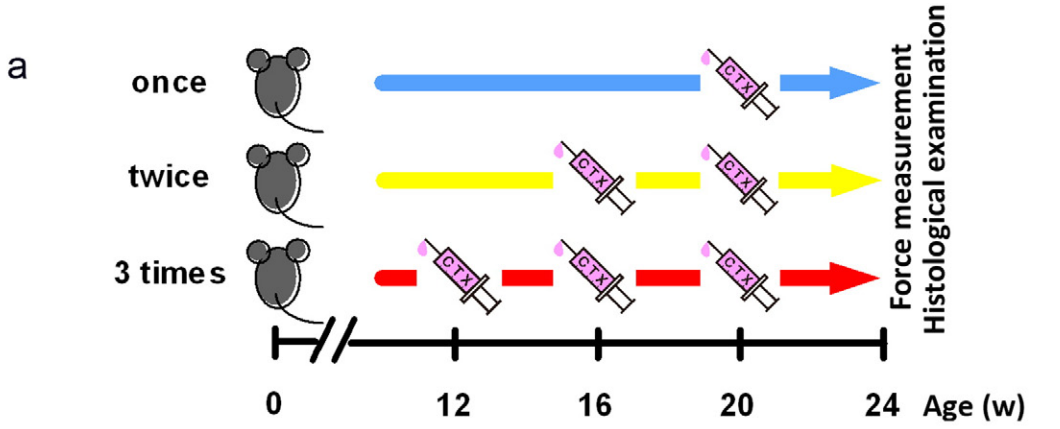
a
once
twice
3 times
CTX
Force measurement
Histological examination
0
12
16
20
24
Age (w)

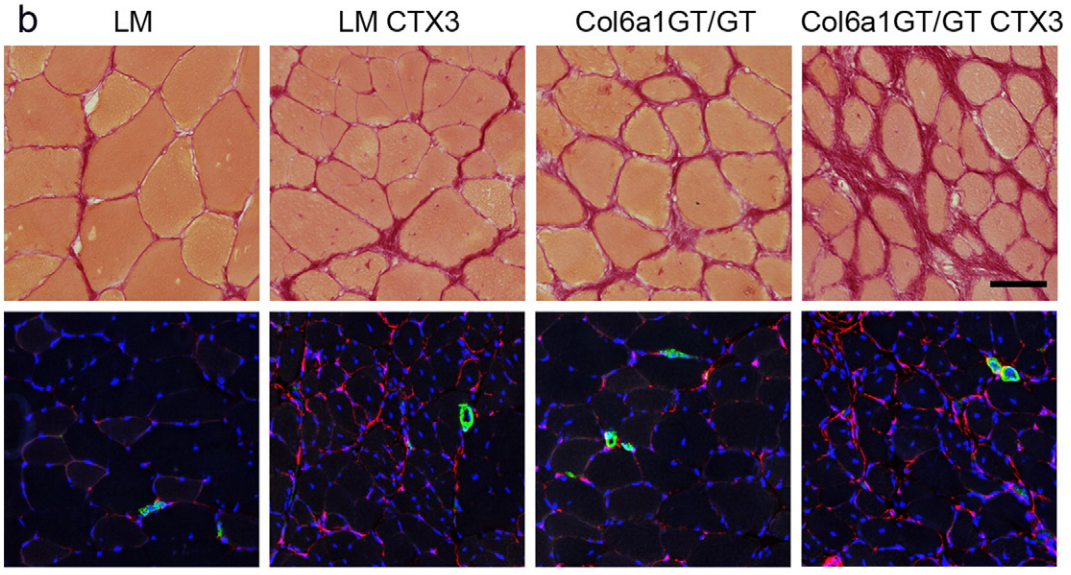
b
LM
LM CTX3
Col6a1GT/GT
Col6a1GT/GT CTX3

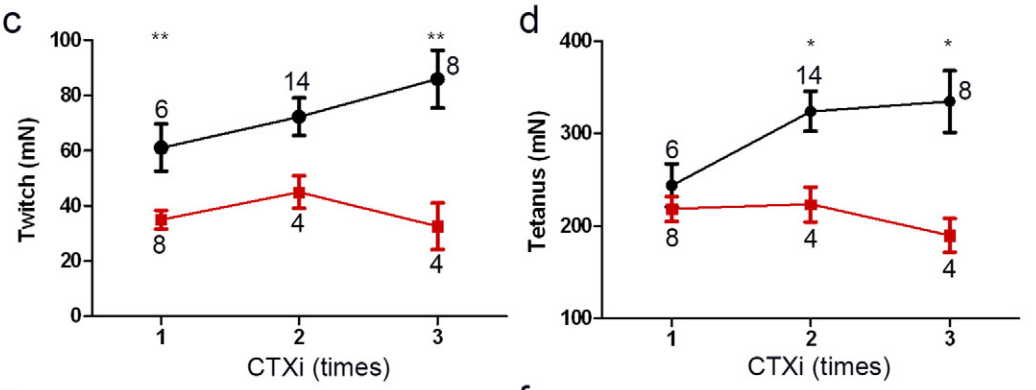
c
Twitch (mN)
CTXi (times)
d
Tetanus (mN)
CTXi (times)

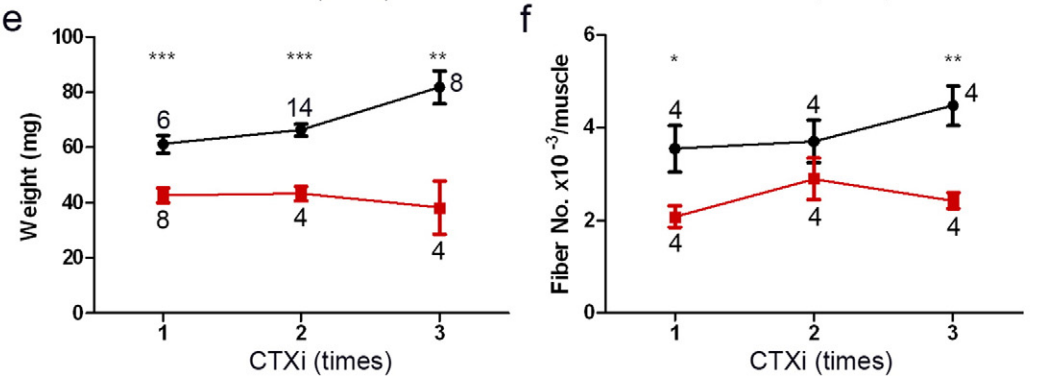
e
Weight (mg)
CTXi (times)
f
Fiber No. x10-3/muscle
CTXi (times)

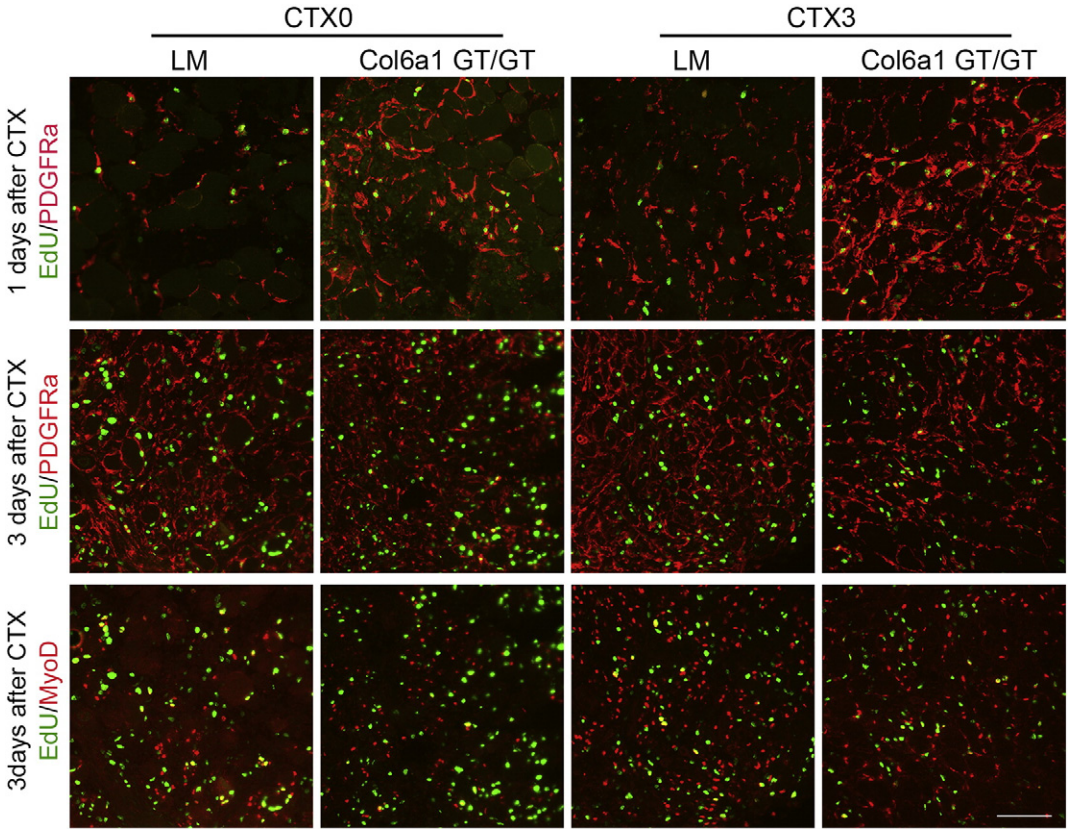

Fig. 7. Activation of MPCs and myoblasts after CTXi. Upper, 1 day after CTXi with EdU (green) and PDGFRα (red) staining; middle, 3 days after CTXi with EdU (green) and PDGFRα (red); bottom, 3 days after CTXi with EdU (green) and MyoD (red). CTX0, no pretreated mice; CTX3, three-times CTX-treated mice. PDGFRα-positive MPCs (red) proliferated rapidly in *Col6a1*$^{GT/GT}$ muscles and repetitive CTXi enhanced their proliferation (red in CTX3) in upper. It is noted that most of proliferating cells are MPCs (nucleus in green and surface in red). On 3 days after CTXi, MyoD-positive myoblasts were similarly proliferating in control LM and *Col6a1*$^{GT/GT}$ muscles in bottom (nuclei in yellow). Bar denotes 100 μm.

muscles in *Col6a1*$^{GT/GT}$ mice. It has been suggested that the MPCs are suppressed by the physical interaction with muscle fibers (Uezumi et al., 2011); it may be conceivable that collagen VI can act as a scaffold to allow interaction between MPCs and myofibers and therefor help maintain normal muscle environment by MPC suppression.

The interaction between satellite cells and MPCs, which are also identified as Tcf4^{+} muscle connective tissue fibroblasts (Murphy et al., 2011), is crucial for muscle regeneration. When muscle necrosis ensues, MPCs lose the interaction with myofibers, hence are activated. In a response to injury, MPCs undergo several steps to initiate a cascade of repair: MPCs phagocytose the necrotic debris and secrete cytokines (IL-6, IGF-1) and ECM proteins; then MPCs assist satellite cells to promote correct myogenic regeneration; after myofiber regeneration, MPCs become inactivated as the amount of connective tissue is diminished (Heredia et al., 2013). During muscle regeneration, ablation of Tcf4^{+} fibroblasts leads to premature satellite cell differentiation, leading to the formation of early regenerating myofibers with smaller diameter at the point of completion of muscle regeneration (Murphy et al., 2011). In contrast, the *Col6a1*$^{GT/GT}$ mice show a remarkable increase in MPCs on 1 day after muscle injury and a persistence of muscle regeneration as large and multiple nucleated myofibers are seen. The number of proliferating satellite cells in *Col6a1*$^{GT/GT}$ muscles, however, was similar to that of normal control. Thus in the absence of collagen VI, the signal (from the myofiber) to suppress MPCs is decreased during muscle necrosis, while during myofiber regeneration, the MPC signals needed to promote induction of satellite cell differentiation are dysregulated. In addition to defects in muscle regeneration, MPCs also contribute to the fibrotic cell population.

Previous studies have implicated impaired autophagy in *Col6a1*$^{-/-}$ muscles, which lead to the inability to degrade degenerated mitochondria, causing permeability transition pore opening and eventually resulting to apoptotic cell death (Grumati et al., 2010; Irwin et al., 2003). In the muscles of our *Col6a1*$^{GT/GT}$ mice, starvation-induced autophagic flux was likewise delayed; there was no accumulation, however, of polyubiquitinated proteins or p62 in muscles (data not shown), both of which are observed in autophagy-deficient mice (Masiero et al., 2009). Furthermore, the pattern of myofiber atrophy was different between *Col6a1*$^{GT/GT}$ and muscle-specific *Atg7*$^{-/-}$ muscles (data not shown). We think that the delay of starvation-induced autophagic flux in *Col6a1*$^{GT/GT}$ muscles is a secondary phenomenon due to metabolic defects as previously suggested (Khan et al., 2009) and not a primary phenomenon.

Our findings in *Col6a1*$^{GT/GT}$ mice provide the insights on therapeutic strategies for UCMD. The muscle weakness *Col6a1*$^{GT/GT}$ mouse is primarily due to small size of skeletal muscles as there is a paucity or almost lack of myofiber necrosis or degeneration. Although the number

Fig. 6. MPC activation by repetitive CTXi in *Col6A1*$^{GT/GT}$ TA muscles. (a) Schedule of the treatment. CTX was injected 1–3 times with a 4-week interval and on 24 weeks of age, muscles were examined by force measurement and histological observation. Control LM (once, $n = 6$; twice, $n = 14$; three times, $n = 8$) and *Col6a1*$^{GT/GT}$ (once, $n = 8$; twice, $n = 4$; three times, $n = 4$) (b) Upper, Sirius red staining; lower, PDGFRα (red), smooth muscle actin (green), DAPI (blue) staining. LM and *Col6a1*$^{GT/GT}$, no treatment of CTXi; LM CTX3 and *Col6a1*$^{GT/GT}$ CTX3, 3 times-CTXi. Bar denotes 50 μm. (c) Peak isometric twitch ($n = 4$–14), (d) maximal tetanic force ($n = 4$–14), (e) muscle weight ($n = 4$–14), (f) total myofiber number in a cross-section ($n = 4$). Data represent mean ± SEM. $^{*}p < 0.05$, $^{**}p < 0.01$, $^{***}p < 0.001$ on the paired *t*-test were used. Numbers in graphs represent *n* for each data point.

of myofibers is reduced, we do not observe prominent myofiber atrophy, suggesting a lack of activation in the atrophy-related signaling. Therefore, therapeutic targets that promote myofiber increase might be useful. Additionally, the observation of selective reduction of twitch force generation in *Col6a1*$^{GT/GT}$ mice suggests inability of myofibers to contract in synchrony; this is likely due to fibrosis in the whole muscle that expands to the interstitial area, disrupting the connection between each myofiber. As such, another therapeutic approach can be aimed at the reduction of MPC-mediated fibrosis through cell transplantation of normal/gene-corrected MPCs or supplementation of collagen VI fibrils into the muscle tissues.

Funding Sources

This study is partially supported by Intramural Research Grant (28-6) for Neurological and Psychiatric Disorders of NCNP, by Comprehensive Research on Disability Health and Welfare from the Ministry of Health, Labor and Welfare (H25-Shinkei Kin-Ippan-004) from Japan Agency for Medical Research and Development, AMED, and by JSPS KAKENHI (JP26293214, JP15H04846). M.C.V.M. is supported by the NHGRI Intramural Research Program of the National Institutes of Health, USA.

Conflicts of Interest

The authors declare no conflicts of interest relevant to what we wrote.

Author Contributions

S.N. designed the research; S.N., M.O., M.C.V.M., and I. Nonaka performed the research; S.N., M.O., M.C.V.M., I. Nonaka and I. Nishino analyzed the data; and S.N., M.O. and M.C.V.M. wrote the paper with inputs from all the authors.

Acknowledgement

The Pax7 antibody developed by Kawakami A. was obtained from the Developmental Studies Hybridoma Bank developed under the auspices of the NICHD and maintained by the University of Iowa, Department of Biology, Iowa City, IA 52242.

Appendix A. Supplementary data

Supplementary data to this article can be found online at http://dx.doi.org/10.1016/j.ebiom.2016.12.011.

References

Allamand, V., Brinas, L., Richard, P., Stojkovic, T., Quijano-Roy, S., Bonne, G., 2011. ColVI myopathies: where do we stand, where do we go? Skelet. Muscle 1, 30.

Angelin, A., Tiepolo, T., Sabatelli, P., Grumati, P., Bergamin, N., Golfieri, C., Mattioli, E., Gualandi, F., Ferlini, A., Merlini, L., et al., 2007. Mitochondrial dysfunction in the pathogenesis of Ullrich congenital muscular dystrophy and prospective therapy with cyclosporins. Proc. Natl. Acad. Sci. U. S. A. 104, 991–996.

Baker, N.L., Morgelin, M., Peat, R., Goemans, N., North, K.N., Bateman, J.F., Lamande, S.R., 2005. Dominant collagen VI mutations are a common cause of Ullrich congenital muscular dystrophy. Hum. Mol. Genet. 14, 279–293.

Bonaldo, P., Braghetta, P., Zanetti, M., Piccolo, S., Volpin, D., Bressan, G.M., 1998. Collagen VI deficiency induces early onset myopathy in the mouse: an animal model for Bethlem myopathy. Hum. Mol. Genet. 7, 2135–2140.

Braghetta, P., Fabbro, C., Piccolo, S., Marvulli, D., Bonaldo, P., Volpin, D., Bressan, G.M., 1996. Distinct regions control transcriptional activation of the alpha1(VI) collagen promoter in different tissues of transgenic mice. J. Cell Biol. 135, 1163–1177.

Braghetta, P., Ferrari, A., Fabbro, C., Bizzotto, D., Volpin, D., Bonaldo, P., Bressan, G.M., 2008. An enhancer required for transcription of the *Col6a1* gene in muscle connective tissue is induced by signals released from muscle cells. Exp. Cell Res. 314, 3508–3518.

Grumati, P., Coletto, L., Sabatelli, P., Cescon, M., Angelin, A., Bertaggia, E., Blaauw, B., Urciuolo, A., Tiepolo, T., Merlini, L., et al., 2010. Autophagy is defective in collagen VI muscular dystrophies, and its reactivation rescues myofiber degeneration. Nat. Med. 16, 1313–1320.

Heredia, J.E., Mukundan, L., Chen, F.M., Mueller, A.A., Deo, R.C., Locksley, R.M., Rando, T.A., Chawla, A., 2013. Type 2 innate signals stimulate fibro/adipogenic progenitors to facilitate muscle regeneration. Cell 153, 376–388.

Higuchi, I., Shiraishi, T., Hashiguchi, T., Suehara, M., Niiyama, T., Nakagawa, M., Arimura, K., Maruyama, I., Osame, M., 2001. Frameshift mutation in the collagen VI gene causes Ullrich's disease. Ann. Neurol. 50, 261–265.

Holt, L.J., Turner, N., Mokbel, N., Trefely, S., Kanzleiter, T., Kaplan, W., Ormandy, C.J., Daly, R.J., Cooney, G.J., 2012. Grb10 regulates the development of fiber number in skeletal muscle. FASEB J. 26, 3658–3669.

Hosaka, Y., Yokota, T., Miyagoe-Suzuki, Y., Yuasa, K., Imamura, M., Matsuda, R., Ikemoto, T., Kameya, S., Takeda, S., 2002. Alpha1-syntrophin-deficient skeletal muscle exhibits hypertrophy and aberrant formation of neuromuscular junctions during regeneration. J. Cell Biol. 158, 1097–1107.

Irwin, W.A., Bergamin, N., Sabatelli, P., Reggiani, C., Megighian, A., Merlini, L., Braghetta, P., Columbaro, M., Volpin, D., Bressan, G.M., et al., 2003. Mitochondrial dysfunction and apoptosis in myopathic mice with collagen VI deficiency. Nat. Genet. 35, 367–371.

Ishikawa, H., Sugie, K., Murayama, K., Awaya, A., Suzuki, Y., Noguchi, S., Hayashi, Y.K., Nonaka, I., Nishino, I., 2004. Ullrich disease due to deficiency of collagen VI in the sarcolemma. Neurology 62, 620–623.

Ito, T., Ogawa, R., Uezumi, A., Ohtani, T., Watanabe, Y., Tsujikawa, K., Miyagoe-Suzuki, Y., Takeda, S., Yamamoto, H., Fukada, S., 2013. Imatinib attenuates severe mouse dystrophy and inhibits proliferation and fibrosis-marker expression in muscle mesenchymal progenitors. Neuromuscul. Disord. 23, 349–356.

Joe, A.W., Yi, L., Natarajan, A., Le Grand, F., So, L., Wang, J., Rudnicki, M.A., Rossi, F.M., 2010. Muscle injury activates resident fibro/adipogenic progenitors that facilitate myogenesis. Nat. Cell Biol. 12, 153–163.

Khan, T., Muise, E.S., Iyengar, P., Wang, Z.V., Chandalia, M., Abate, N., Zhang, B.B., Bonaldo, P., Chua, S., Scherer, P.E., 2009. Metabolic dysregulation and adipose tissue fibrosis: role of collagen VI. Mol. Cell. Biol. 29, 1575–1591.

Malicdan, M.C., Noguchi, S., Hayashi, Y.K., Nonaka, I., Nishino, I., 2009a. Prophylactic treatment with sialic acid metabolites precludes the development of the myopathic phenotype in the DMRV-hIBM mouse model. Nat. Med. 15, 690–695.

Malicdan, M.C., Noguchi, S., Nishino, I., 2009b. Monitoring autophagy in muscle diseases. Methods Enzymol. 453, 379–396.

Masiero, E., Agatea, L., Mammucari, C., Blaauw, B., Loro, E., Komatsu, M., Metzger, D., Reggiani, C., Schiaffino, S., Sandri, M., 2009. Autophagy is required to maintain muscle mass. Cell Metab. 10, 507–515.

Mathew, S.J., Hansen, J.M., Merrell, A.J., Murphy, M.M., Lawson, J.A., Hutcheson, D.A., Hansen, M.S., Angus-Hill, M., Kardon, G., 2011. Connective tissue fibroblasts and Tcf4 regulate myogenesis. Development 138, 371–384.

Murphy, M.M., Lawson, J.A., Mathew, S.J., Hutcheson, D.A., Kardon, G., 2011. Satellite cells, connective tissue fibroblasts and their interactions are crucial for muscle regeneration. Development 138, 3625–3637.

Nonaka, I., Une, Y., Ishihara, T., Miyoshino, S., Nakashima, T., Sugita, H., 1981. A clinical and histological study of Ullrich's disease (congenital atonic-sclerotic muscular dystrophy). Neuropediatrics 12, 197–208.

Norwood, F.L., Harling, C., Chinnery, P.F., Eagle, M., Bushby, K., Straub, V., 2009. Prevalence of genetic muscle disease in Northern England: in-depth analysis of a muscle clinic population. Brain 132, 3175–3186.

Okada, M., Kawahara, G., Noguchi, S., Sugie, K., Murayama, K., Nonaka, I., Hayashi, Y.K., Nishino, I., 2007. Primary collagen VI deficiency is the second most common congenital muscular dystrophy in Japan. Neurology 69, 1035–1042.

Uezumi, A., Fukada, S., Yamamoto, N., Takeda, S., Tsuchida, K., 2010. Mesenchymal progenitors distinct from satellite cells contribute to ectopic fat cell formation in skeletal muscle. Nat. Cell Biol. 12, 143–152.

Uezumi, A., Ito, T., Morikawa, D., Shimizu, N., Yoneda, T., Segawa, M., Yamaguchi, M., Ogawa, R., Matev, M.M., Miyagoe-Suzuki, Y., et al., 2011. Fibrosis and adipogenesis originate from a common mesenchymal progenitor in skeletal muscle. J. Cell Sci. 124, 3654–3664.

Ullrich, O., 1930. Congential, atonic-sclerotic muscle dystrophy, a further type of heredodegenerative diseases of the neuro muscular system. Z. Gesamte Neurol. Psychiatry 126, 171–201.

Vecchione, A., Marchese, A., Henry, P., Rotin, D., Morrione, A., 2003. The Grb10/Nedd4 complex regulates ligand-induced ubiquitination and stability of the insulin-like growth factor I receptor. Mol. Cell. Biol. 23, 3363–3372.

Yonekawa, T., Komaki, H., Okada, M., Hayashi, Y.K., Nonaka, I., Sugai, K., Sasaki, M., Nishino, I., 2013. Rapidly progressive scoliosis and respiratory deterioration in Ullrich congenital muscular dystrophy. J. Neurol. Neurosurg. Psychiatry 84, 982–988.

Yonekawa, T., Malicdan, M.C., Cho, A., Hayashi, Y.K., Nonaka, I., Mine, T., Yamamoto, T., Nishino, I., Noguchi, S., 2014. Sialyllactose ameliorates myopathic phenotypes in symptomatic GNE myopathy model mice. Brain 137, 2670–2679.